Noninvasive theranostic imaging of HSV-TK/GCV suicide gene therapy in liver cancer by folate-targeted quantum dot-based liposomes

Shao, D.; Li, J.; Pan, Y.; Zhang, X.; Zheng, X.; Wang, Z.; Zhang, M.; Zhang, H.; Chen, L.

DOI
10.1039/c5bm00077g

Publication date
2015

Document Version
Final published version

Published in
Biomaterials Science

Biomaterials Science

PAPER

View Article Online
View Journal | View Issue

Cite this: *Biomater. Sci.*, 2015, **3**, 833

Noninvasive theranostic imaging of HSV-TK/GCV suicide gene therapy in liver cancer by folate-targeted quantum dot-based liposomes†

Dan Shao,‡[a] Jing Li,‡[a] Yue Pan,[a] Xin Zhang,[a] Xiao Zheng,[a] Zheng Wang,[a] Ming Zhang,[a] Hong Zhang*[b] and Li Chen*[a,c]

Received 12th March 2015,
Accepted 30th March 2015

DOI: 10.1039/c5bm00077g

www.rsc.org/biomaterialsscience

Theranostics is emerging as a popular strategy for cancer therapy; thanks to the development of nanotechnology. In this work, we have combined an HSV-TK/GCV suicide gene system and near-infrared quantum dots, as the former is quite effective in liver cancer treatment and the latter facilitates tumor imaging. A folate-modified theranostic liposome (FL/QD-TK) was developed, which is composed of an HSV-TK suicide gene covalently coupling with near-infrared fluorescent CdSeTe/ZnS core/shell quantum dots. The liver cancer-targeting and biosafety of FL/QD-TK were studied *in vitro* and *in vivo*. FL/QD-TK exhibited highly specific tumor imaging and strong inhibition of the folate receptor-overexpressed Bel-7402 mouse xenografts without systematic toxicity. This study may shed light on gene delivery and targeted cancer therapy.

1. Introduction

Hepatocellular carcinoma (HCC) has been the second leading cause of cancer-related deaths worldwide over the recent decade; despite the mainstay strategies, such as surgery, liver transplantation and chemotherapy, the overall survival of patients with HCC remains unsatisfactory because of the delayed definite diagnosis and the high rate of recurrence and metastasis.[1–3] Hence, there is a pressing need for early diagnostic techniques and effective therapy for HCC. Recently, the term "theranostic" has appeared, which is defined as a material that combines the modalities of therapy and diagnostic imaging agents simultaneously within the same dose.[4–7] Inorganic or organic nanoparticles as drug carriers and imaging agents have made theranostics a promising strategy for HCC treatment.

Among various cancer gene therapy approaches, suicide gene therapy seems to be effective, with bystander effect characteristics.[8,9] Herpes simplex virus thymidine kinase gene (HSV-TK) with ganciclovir (GCV) as a pro-drug is extensively studied and applied in several clinical trials for HCC.[10–12] However, the potential systemic side effects limited its clinical applications because of the TK gene entering into normal tissue and inducing production of toxic GCV triphosphate along with long-term administration of GCV.[11,13,14] Therefore, how to specifically target the tumor tissue or cell is a very important and urgent issue for the HSV-TK/GCV system in HCC therapy.

Cationic liposomes are among the most promising nanometer-scale systems that are used to deliver drugs, genes and proteins, as well as imaging agents.[15–17] For targeted delivery to HCC, cationic liposomes could link with folate because the folate receptor (FR) has been identified as a marker for some types of hepatocellular carcinomas.[18,19] Liposomes conjugated to a folate ligand *via* a polyethylene glycol (PEG) spacer have been successfully used for gene targeted therapy in cancer.[20,21] Moreover, gene therapy guided by molecular imaging enables the improvement of the efficacy and safety of the current gene therapy.[22,23] Molecular imaging is based on specific probes or contrast agents that allow either direct or indirect spatio-temporal evaluation of gene expression, progression, and regression of cancer, as well as targeted therapies.[24–26] Among the currently available contrast agents used in molecular imaging, semiconductor quantum dots (QDs) are popular optical probes in biolabeling and bioimaging applications because of their considerable advantages over conventional organic fluorophores, including tunable emission from visible to infrared wavelengths by varying the size and composition,

[a]*Department of Pharmacology, Nanomedicine Engineering Laboratory of Jilin Province, College of Basic Medical Sciences, Jilin University, Changchun 130021, China. E-mail: chenl@jlu.edu.cn*
[b]*Van't Hoff Institute for Molecular Sciences, University of Amsterdam, Science Park 904, 1098 XH Amsterdam, The Netherlands. E-mail: h.zhang@uva.nl*
[c]*School of Nursing, Jilin University, Changchun 130021, China*
†Electronic supplementary information (ESI) available: Further experimental details and figures, cell imaging and cell viability of FL/QD-TK. See DOI: 10.1039/c5bm00077g
‡These authors contributed equally.

brightness intensity, photostability, broad excitation spectra, and high resistance to photobleaching.[27–32] Recently, QDs have been made into multifunctional platforms integrating tracing and gene delivery functions.[33–35] However, it is necessary to develop strategies to deliver QDs across the cell membrane and to enable subsequent distribution to specific biological targets with both high selectivity and efficiency.

Herein, we aim to design folate-targeted theranostic liposomes, coined as FL/QD-TK, combining the HSV-TK suicide gene and near-infrared fluorescent CdSeTe/ZnS core/shell quantum dots for *in vivo* HCC targeted imaging and improved drug delivery efficiency. The targeted delivery, cellular internalization, and anticancer activity of FL/QD-TK are assessed with FR-overexpression hepatoma cell lines and low FR-expression cell lines. *In vivo* NIR fluorescence imaging, bio-distribution, biocompatibility and blocking studies are performed in Bel-7402 tumor-bearing nude mice.

2. Experimental section

2.1. Materials

Qdot 800 ITK® carboxyl QDs were supplied by Invitrogen Corporation Institute (Carlsbad, CA, Q21371MP, 8 μM solution). QD have a core of CdSeTe and a shell of ZnS. 1-Ethyl-3-(3-dimethylaminopropyl) carbodiimide hydrochloride (EDC, purity 99%), sulfo-*N*-hydroxysulfosuccinimide (sulfo-NHS, purity 98.5%), ethidium bromide (EB) and agarose gel were purchased from Sigma-Aldrich. RPMI-1640 medium and 3-(4,5-dimethylthiazol-2-yl)-2,5-diphenyl tetrazolium bromide (MTT) were obtained from GIBCO. Diagnostic kits for aspartate aminotransferase (AST), alanine aminotransferase (ALT), and blood urea nitrogen (BUN) were purchased from Nanjing Jiancheng Bioengineering Institute. [1,2-Dipalmitoyl-*sn*-glycero-3-phosphocholine(DPPC),3-(*N*-(*N*′,*N*′-dimethyl amino ethane) carbamoyl) cholesterol (DC-cho1), 2-distearoyl-*sn*-glycero-3-phosphor ethanolamine-*N*-[methoxy(polyethylene glycol)-2000] (DSPE-PEG2000) and 1,2-distearoyl-*sn*-glycero-3-phosphoethanolamine-*N*-[folate (polyethylene glycol)-2000]-(DSPE-PEG2000-folate) were purchased from Avanti Polar Lipids (Alabaster, AL). Deionized water was purified through a Milli-Q water purification system, and the resistivity was 18.2 MΩ cm. pCMV-TK encoding the HSV-TK gene under the control of the CMV promoter was kindly presented by Dr You-Sub Won (Department of Molecular Biology, Institute of Nanosensor and Biotechnology, Dankook University).

2.2 FL/QD-TK preparation

QD-TK conjugates were synthesized and purified according to the method reported previously.[36] Multifunctional liposomes with lipids (20 mg) at a DPPC : DC-chol : DSPE-PEG2000 : DSPE-PEG2000-folate (60 : 30 : 9.5 : 0.5) molar ratio through the thin film hydration method were prepared under the conditions of chloroform–methanol (3 : 1) in a round-bottom flask. The solvent was evaporated using a rotary evaporator to form a thin layer of lipids under a vacuum for 30 min at 40 °C and then flushed with a N_2 stream to remove any residual traces of the organic solvent. The dried lipid film was initially dissolved with 2 mL PBS into a QD-TK suspension; FL/QD-TK hybrids were prepared by bath sonication for 10 min at 30 °C. As a control, non-targeted liposomes (L/QD-TK) were also prepared according to the same procedure.

2.3 FL/QD-TK characterization

Size distribution and zeta potential were measured by laser light scattering using a Zetasizer (Nano ZS, Malvern Instruments, Malvern, UK) after water dispersion. Transmission electron microscopy (TEM) images were obtained with a JEM-2100F transmission electron microscope (JEOL, Ltd, Japan) at a 200 kV accelerating voltage. Samples for TEM analysis were prepared by depositing a drop of the micelle solution (10 μL, 0.5 mg mL^{-1}) onto carbon-coated copper grids and then by drying at room temperature. The morphology and composition of the nanoparticles were inspected using a scanning electron microscope (FESEM, S4800, Hitachi). Ultraviolet-visible (UV-vis) absorption and fluorescence emission spectra were measured at room temperature by a UV-3101 spectrophotometer and a Hitachi F-4500 fluorescence spectrofluorimeter, respectively. To evaluate the QD-TK conjugate loading ability of liposomes, the agarose gel electrophoresis was carried out with a Bio-Rad imaging system; the QD-TK conjugates, L/QD-TK and FL/QD-TK were characterized by the agarose gel (0.8% w/v) electrophoresis technique, and agarose gel electrophoresis was run at 120 V cm^{-1} for 20 min.

2.4 Cell culture and tumor-targeting evaluation by cell imaging

FR-overexpression human hepatoma cell lines, including Bel-7402, Hep3B and SMMC-7721, and low FR-expression human hepatoma cell lines HepG2 and HL-7702 human hepatic embryo cells were obtained from ATCC. All cells were maintained in a high glucose Dulbecco's modification of Eagle's medium (DMEM) supplemented with 10% fetal bovine serum, 100 units mL^{-1} penicillin, and 100 mg mL^{-1} streptomycin. The cells were seeded in 24-well plates at a density of 1×10^5 cells per well and were routinely incubated overnight at 37 °C. FL/QD-TK or L/QD-TK solution was added to the culture medium and both reached the final concentration of 12.5 μg mL^{-1}. In the free folate competition assay, folate with a final concentration of 1 mM was co-cultured with 12.5 μg mL^{-1} FL/QD-TK for 6 h. The cells were washed twice with chilled PBS and the nuclei were stained with Hoechst 33258 (5 μg mL^{-1}) for 5 min. Cell imaging was observed by using an Olympus FV1000 confocal laser scanning microscope equipped with a multi-line argon LASER, 405, 488 nm, and a 30 mW Laser class 3D laser.

2.5 Cell viability assay

Cells were seeded at a density of 6×10^3 cells per well in 96-well plates overnight, and then the cells were treated with different concentrations of FL/QD-TK or L/QD-TK for 96 h to determine the safety dose of the nanocarrier. To investigate

the antitumor efficacy of liposomes, FL/QD-TK or L/QD-TK with a dose of 12.5 μg mL^{-1} were co-cultured with cells 24 h prior to the addition of GCV (10 μg ml^{-1}). An MTT assay was conducted in 96-well plates in triplicate after GCV treatment for 24, 48 or 72 h. The optical density (OD) value was measured by using a microplate reader (Sanyo Company) at 570 nm.

2.6 *In vivo* mice xenograft model, tumor and tissue distribution imaging

Animal experiment protocols were approved by the Ethics Committee for the Use of Experimental Animals of Jilin University. Bel-7402 cells (2×10^5) were collected in 70 μL PBS and mixed with 70 mL Matrigel Matrix (Becton Dickinson Biosciences). The mixture was injected subcutaneously on one side of the dorsal flank of 8-week-old male BALB/c nu/nu mice (Vital River Laboratories, Beijing, China). In *in vivo* tumor imaging and *ex vivo* tissue distribution experiments, the mice with a Bel-7402 xenograft after a 4-week inoculation were used and treated with FL/QD-TK (50 mg kg^{-1}) and L/QD-TK (50 mg kg^{-1}), respectively, by a one-time tail vein injection. The mice were anesthetized and imaged at designed intervals (0.5, 2, 6 and 24 h) after post-injection. The dynamic tumor images were monitored by the Xenogen IVIS Spectrum system using Living Imaging software (Cambridge Research Instrumentation; Woburn, MA, excitation: 640 ± 30 nm, emission: 760 nm long pass).

To confirm the *in vivo* distribution of FL/QD-TK or L/QD-TK, the mice were sacrificed 24 h post-injection. The tumor and major organs (heart, liver, spleen, lung, and kidney) were removed and imaged by the NIR imaging system. NIR fluorescence intensity at the ROI is expressed as the mean ± SD for three mice in each group. Moreover, all the tissues were immediately frozen and prepared into 4 μm sections, and then the sections were soaked in cold acetone for 3 min, rinsed with PBS for 15 min at room temperature following nuclear staining by Hoechst 33258. Fluorescence visualization of the tumor and tissues was performed by CLSM.

2.7 *In vivo* antitumor efficacy in Bel-7402 xenograft mice

The mouse Bel-7402 xenograft model was replicated as mentioned above. When the tumor volumes reached 60–100 mm^3, the mice were randomized into 6 groups (n = 5) and treated with saline, GCV (50 mg kg^{-1}), L/QD-TK (50 mg kg^{-1}), FL/QD-TK (50 mg kg^{-1}), L/QD-TK (50 mg kg^{-1}) plus GCV (50 mg kg^{-1}), and FL/QD-TK (50 mg kg^{-1}) plus GCV (50 mg kg^{-1}), respectively, by tail vein injection every 3 to 4 days. The injections were repeated six times over a 26-day treatment period. The pre-drug GCV (50 mg kg^{-1}) was injected intraperitoneally every other day after the first injection of L/QD-TK or FL/QD-TK. The body weights and tumor sizes were recorded once every three days and the tumor volumes were calculated according to the formula: length × $width^2$ × 0.52. The mice were sacrificed 26 days after implantation of the tumor cells.

2.8 Systemic safety evaluation

When the mice were sacrificed on the 26th day, all tumors and major organs (heart, liver, spleen, lung, and kidney) were removed and weighed. Serum was collected after centrifuging the whole blood at 3000 rpm for 15 min. The biochemical parameters, including alanine aminotransferase (ALT), aspartate aminotransferase (AST), glucose (GLU) and blood urea nitrogen (BUN) were assayed with diagnostic kits from Nanjing Jiancheng Bioengineering Institute. In addition, the tissues including tumors, livers, kidneys, spleens, lungs, and hearts were fixed in 10% formalin and then embedded into paraffin. Four μm tissue sections were made and stained with hematoxylin–eosin (H&E). The safety evaluation based on pathological changes in tissues was conducted by an experienced veterinary pathologist.

2.9 Statistical analysis

The data are expressed as the means ± SD. The statistical significance of the data was compared by Student's t-test. Analysis of variance (ANOVA) was used to analyze the differences among the different groups.

3. Results and discussion

3.1 Synthesis and characterization of FL/QD-TK

We successfully synthesized QD-TK conjugates and demonstrated the stable linkage between near-infrared fluorescent CdSeTe/ZnS core/shell quantum dots and the HSV-TK suicide gene. To achieve high gene transfection efficiency and targeting *in vivo*, folate-modified lipid FA-PEG-DSPE was employed in the total lipid during self-assembly preparation. To this end, folate-targeted liposomes (FL/QD-TK) were prepared using well-established liposome preparation protocols to encapsulate QD-TK conjugates, and the characterization of FL/QD-TK was determined.

As shown in Fig. 1a, a transmission electron microscopy (TEM) image of FL/QD-TK showed a wide distribution of the individual QDs with a size of 5 nm; the incorporation of hydrophilic QDs resulted in a rough particle surface. It is worth noting that multiple QDs were localized in the liposomes and can be visualized. Scanning electron microscopy (SEM) observation showed that FL/QD-TK possessed a uniform small size of approximately 100 nm or greater, with a nearly spherical shape, which may be prone to exhibit longer circulation time and be taken up more easily by cancer cells, as shown in Fig. 1b. Moreover, the particle size distribution and zeta potential of FL/QD-TK are shown in Fig. 1c and d; the aqueous dispersion of FL/QD-TK alone exhibited an average particle size of 89.7 ± 3.3 nm and a positive surface charge (+20.1 ± 1.4 mV), which was consistent with electron microscopy observations.

The fluorescence emission spectra of FL/QD-TK are shown in Fig. 1e; the strong PL at a near-infrared region from the FL/QD-TK aqueous solution demonstrated that FL/QD-TK contained a large number of QDs, while a little reduction in intensity was observed after incorporation. Notably, a slight red

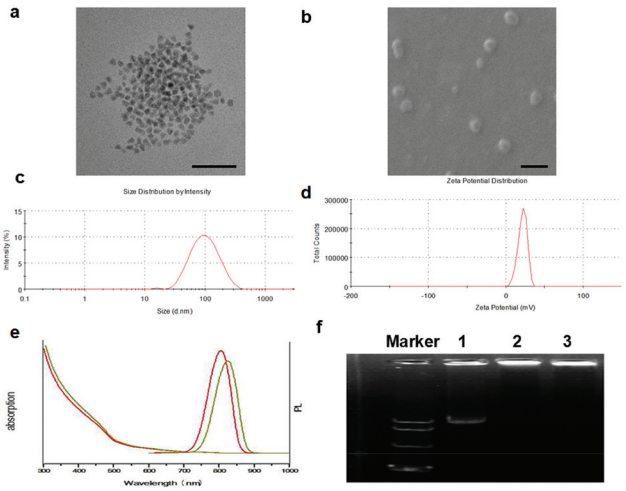

Fig. 1 Characterization of FL/QD-TK. (a) TEM images of FL/QD-TK, scale bars are 50 nm. (b) SEM images of FL/QD-TK, scale bars are 200 nm. (c) Dynamic-light scattering showed that the mean diameter of these nanoparticles is approximately 90 nm. (d) Zeta potential measurements showed that the zeta potential of FL/QD-TK is approximately +20 V. (e) UV-vis absorbance and photoluminescence emission spectra of QDs (yellow line) and FL/QD-TK (red line). (f) Agarose gel electrophoresis of lane (1) QD-TK conjugates, (2) L/QD-TK and (3) FL/QD-TK.

shift of the PL peak was observed in the FL/QD-TK solution compared to that of the pure QD-TK conjugates solution, probably because of the interaction between the positive charges of the inner surface of the liposome vesicles and negative charges on the free carboxyl groups of the QD surface.

Formation of stable complexes between a vector and the DNA is an important prerequisite for efficient gene delivery.[37,38] Fig. 1f displays the agarose gel electrophoresis patterns of the QD-TK conjugates, L/QD-TK and FL/QD-TK. It was shown that L/QD-TK and FL/QD-TK could completely retard plasmid DNA, indicating that all the cationic liposomes condensed DNA efficiently. In addition, we found that the photoluminescence, average particle size and zeta potential of FL/QD-TK were not significantly changed after storage in PBS at 4 °C for 30 days (data not shown), indicating that FL/QD-TK exhibited good photostability and storage stability.

3.2 Folate-modification enhanced the tumor targeting

The overexpression of the folate receptor (FR) on tumor cells makes this glycoprotein an attractive and effective target for site-specific delivery of antitumor drugs into proliferating cells.[39,40] Folate–drug conjugates, folate–polyplex, folate-modified liposomes, micelles, or dendrimers have been widely utilized in target therapy for disease treatment.[41,42] Herein, three liver cancer cell lines with folate receptor (FR) overexpression, including Bel-7402, Hep3B and SMMC-7721, were selected, and two cell lines with low FR-expression, including HepG2 human hepatoma cells and HL-7702 human hepatic embryo cells, were employed for a comparative study. QD fluorescence in five cell lines was determined by confocal microscopic analysis after co-culture with FL/QD-TK alone or L/QD-TK alone, and the folate receptor blocking groups prior to adding free folic acid. As shown in Fig. 2–4 and Fig. S1,† QD fluorescence in Bel-7402, Hep3B and SMMC-7721 cells with FR overexpression was much higher in the treatment of FL/QD-TK compared to the L/QD-TK treatment. There was no difference in QD fluorescence between the FL/QD-TK and L/QD-TK groups in the FR-low expression HepG2 and HL-7702 cells. Furthermore, FR-enriched Bel-7402 cells incubated with 12.5 μg ml^{-1} of FL/QD-TK for 6 h showed stronger QDs fluorescence; however, this strong fluorescence was significantly attenuated prior to

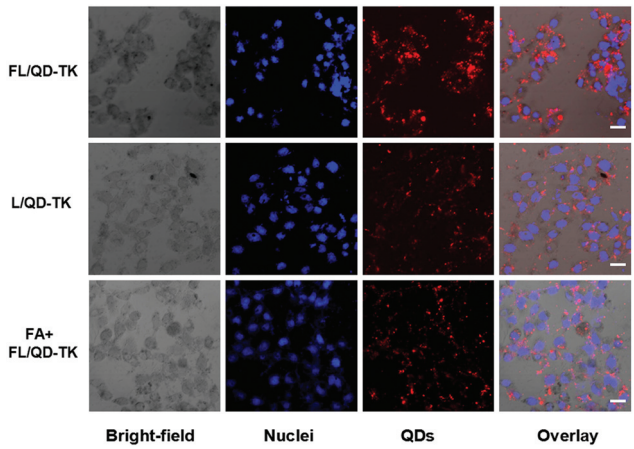

Fig. 2 Cell uptake of FL/QD-TK in Bel-7402 cells. Laser confocal scanning microscopic images of folate receptor positive Bel-7402 cells incubated with the targeted liposome FL/QD-TK, non-targeted liposome L/QD-TK and FL/QD-TK + FA. Red florescence: quantum dots, nuclei: stained blue with Hoechst 33342. Scale bars are 10 μm.

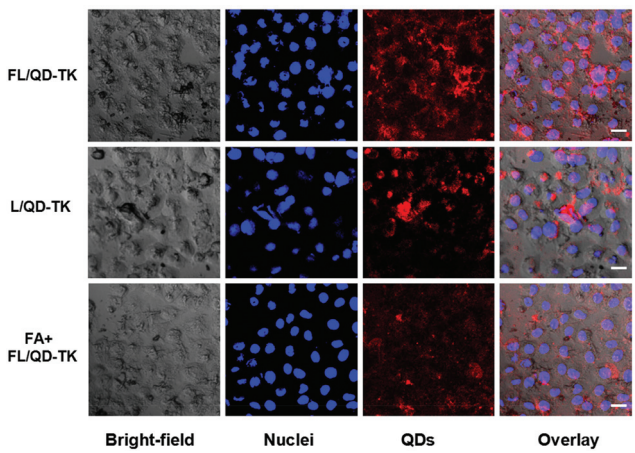

Fig. 3 Celluptake of FL/QD-TK in Hep3B cells. Laser confocal scanning microscopic images of folate receptor positive Hep3B cells incubated with the targeted liposome FL/QD-TK, non-targeted liposome L/QD-TK and FL/QD-TK + FA. Red florescence: quantum dots, nuclei: stained blue with Hoechst 33342. Scale bars are 10 μm.

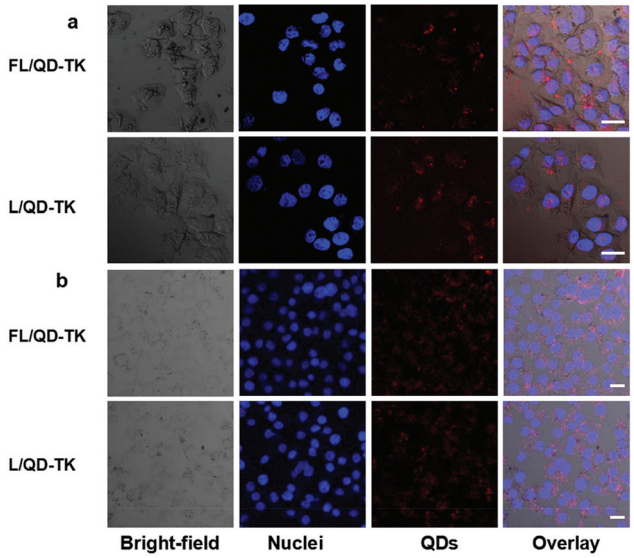

Fig. 4 Cell uptake of FL/QD-TK in HL-7702 and HepG2 cells: Laser confocal scanning microscopic images of folate receptor negative HL-7702(a) and HepG2(b) cells incubated with targeted liposome FL/QD-TK and non-targeted liposome L/QD-TK. Red florescence: quantum dots, nuclei: stained blue with Hoechst 33342. Scale bars are 10 μm.

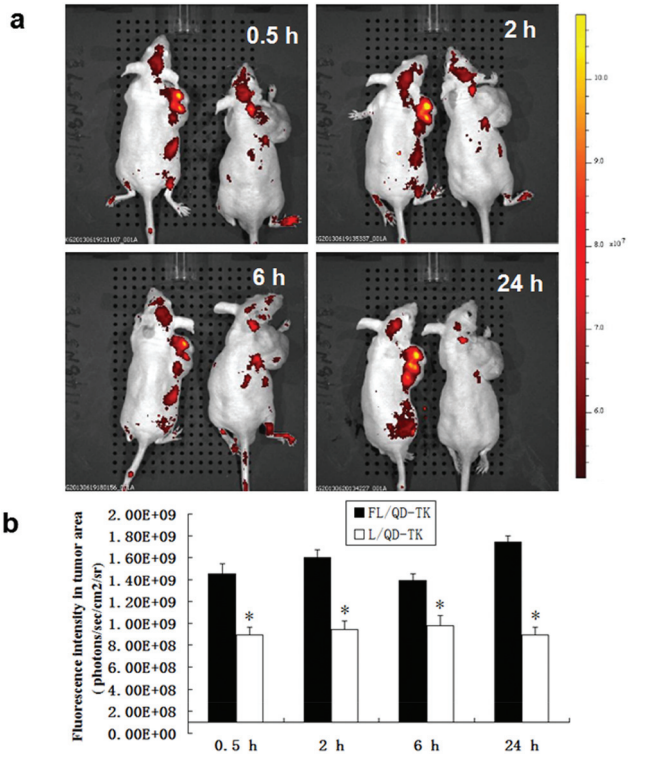

Fig. 5 Real-time imaging of FL/QD-TK in Bel-7402 tumor xenograft model. (a) *In vivo* QD fluorescence images showing folate-enhanced tumor targeting of the FL/QD-TK or L/QD-TK after tail vein injection into nude mice bearing Bel-7402 subcutaneous xenografts at different times. (b) Fluorescence intensity at the tumor site for up to 24 hours. Mean values ± SD. $*P < 0.05$ stands for FL/QD-TK *versus* L/QD-TK group.

addition of exogenous free folate. Similar phenomena were observed in Hep3B cells and SMMC-7721 cells. These results demonstrated that free folic acid could compete with FL/QD-TK on FR and subsequently inhibit the internalization of FL/QD-TK, which indicated that the folate modified QD/TK indeed enhanced the tumor target.

3.3 FL/QD-TK imaging and tissue distribution *in vivo*

FL/QD-TK exhibited targeted gene delivery in FR-overexpression Bel-7402 liver cancer cells *in vitro*. However, whether FL/QD-TK could become a promising imaging probe *in vivo* conditions remains unknown. Therefore, the real-time *in vivo* fluorescence images were investigated using a Bel-7402-bearing nude mouse model. L/QD-TK and FL/QD-TK were respectively injected to Bel-7402-bearing mice in the tail vein with a dose of 50 mg kg^{-1}, and then images were taken at various time points (0.5, 2, 6 and 24 h) by the NIR imaging system. Representative images are shown in Fig. 5, the left mouse with FL/QD-TK in each panel displayed strong red QDs fluorescence localized only in the tumor site from the initial administration at 0.5 h to the last time point at 24 h. In contrast to the right mouse with L/QD-TK, there was no red fluorescence in the tumor site. This confirmed that the folate modification enhanced the tumor targeting *in vivo* and *in vitro*. Interestingly, the fluorescence signals for the FL/QD-TK gradually increased at the tumor site until 24 h, and the remaining NIR fluorescence were observed even on the 7th day post-injection (data not shown), implying that FL/QD-TK had an accumulated effect in the tumor and a long half-life *in vivo*.

To verify the *in vivo* biodistribution of FL/QD-TK, the whole tumor as well as major organs, such as liver, spleen, lung, kidney, brain, and heart were removed after 24 h for a one time injection in the tail vein, and *ex vivo* NIR fluorescence images were obtained immediately. As shown in Fig. 6a, the tumor tissue in FL/QD-TK-treated mice had the highest fluorescence signal compared to other organs, while the tumor tissue in L/QD-TK-treated mice has almost the same fluorescence intensity as other organs. A quantitative analysis of the fluorescence intensity in tumor tissue in the FL/QD-TK group showed it to be significantly higher than in the L/QD-TK group (Fig. 6b). Moreover, cryo-sections of the tumor and organ were prepared and imaged (Fig. 6c). FL/QD-TK could attain higher intratumoral cellular uptake and spread extensively within tumor tissues than L/QD-TK, implying that increased internalization of the TK gene within tumor cells occurred not only *in vitro* but also *in vivo*, which was in good agreement with real-time *in vivo* imaging and *ex vivo* organ imaging results. In addition, median signals were optically visualized by using the NIR imaging system in the liver, spleen and kidney both in FL/QD-TK and L/QD-TK treated mice. Herein, we had to take into account the question between optical imaging and probe distribution *in vivo* because blood

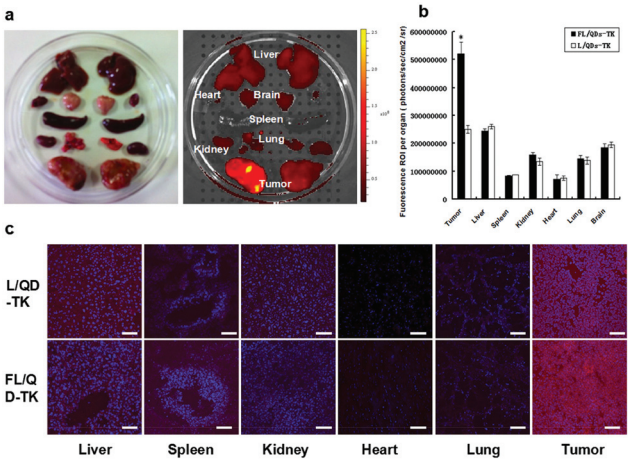

Fig. 6 Biodistribution of FL/QD-TK in the Bel-7402 tumor xenograft model. (a) Tissue distribution of L/QD-TK and FL/QD-TK in Bel-7402 tumor-bearing mice. 24 hours after intravenous administration of NPs, tissues were harvested and NIR fluorescence signals were measured by IVIS imaging. The strength of the signals is shown in the side bar. (b) Biodistributions of L/QD-TK and FL/QD-TK based on the fluorescence intensity of NIR QDs signal (n = 3). Mean values ± SD. *P < 0.05 stands for FL/QD-TK *versus* L/QD-TK group. (c) Confocal microscopic imaging of tissue sections was taken from heart, spleen, kidney, lung and liver. Scale bars are 100 μm.

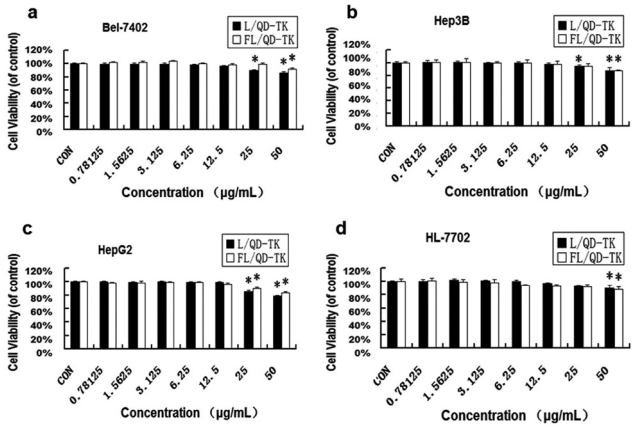

Fig. 7 Effect of FL/QD-TK on cell viability. Cell viability in Bel-7402 cell (a), Hep3B cell (b), HepG2 (c) and HL-7702 (d) during 96 h-treatment with different concentrations of FL/QD-TK and L/QD-TK measured by the MTT assay. The data represent three separate experiments. Mean values ± SD. *P < 0.05 *versus* control group.

strongly absorbed NIR light and thus, significantly reduced the measured fluorescence. Therefore, based on the relative abundance of blood volumes in the liver and spleen, the accumulation of the probe in these organs was most likely underestimated.[43] Furthermore, the distribution of FL/QD-TK in the liver and spleen represented the elimination capacity of the reticuloendothelial system, which embodied, to some extent, the bio-capability and immunogenicity of FL/QD-TK.[44,45] Overall, these results indicated that FL/QD-TK has great feasibility and practicability for *in vivo* tumor-targeted real-time imaging and for tracing the temporal and spatial distribution of the TK gene, which shows potential for use as a suicide gene carrier or as an optical imaging agent for cancer diagnosis.

3.4 The theranostic application of FL/QD-TK/GCV *in vitro* and *in vivo*

It is well known that cadmium-based QDs are often associated with significant cytotoxicity, which has been widely discussed over the past few years. Therefore, it is very important to evaluate the cytotoxicity of the QD-based liposomes used as gene delivery carriers. Cell viabilities were evaluated by the MTT assay after co-culture with FL/QD-TK and L/QD-TK in Bel-7402, Hep3B, SMMC-7721, HL-7702 and HepG2 cells. As shown in Fig. 7 and Fig. S2,† cell viability remained higher than 95% for a 96 h co-culture with both liposomes when the concentrations were less than 12.5 μg mL^{-1}, which revealed that 12.5 μg mL^{-1} QD-based liposomes were virtually non-toxic and safe as a gene drug delivery carrier.

The TK gene is a suicide gene that converts pre-drug GCV into a toxic phosphorylated form, inhibits DNA polymerase and/or incorporates into the DNA, finally causing DNA chain termination and tumorcell death.[46,47] Importantly, this cytotoxic compound could have "bystander effects," meaning that it could increase the number of apoptotic cells compared with the number of cells transduced, minimizing the necessity of transfecting 100% of tumor cells and improving therapeutic efficacy.[48,49] In the present study, GCV was given as a single dose at the final concentration of 10 μg mL^{-1} following a 24 h coculture with 12.5 μg mL^{-1} of L/QD-TK or FL/QD-TK, and then cell viability was measured by the MTT assay at 24, 48, or 72 h after GCV administration. As depicted in Fig. 8 and Fig. S3,† the tumor cell killing effect was achieved in either

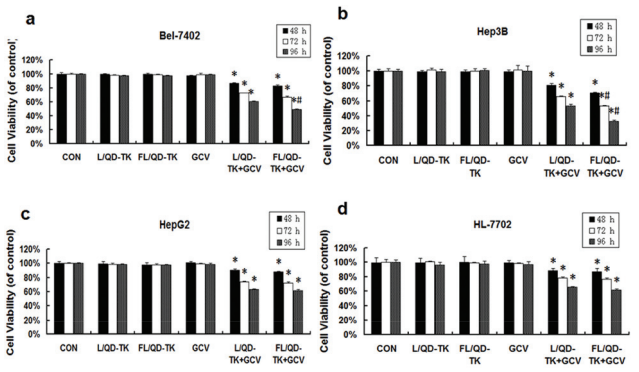

Fig. 8 Antitumor effect of FL/QD-TK plus GCV on cell viability. Cell viability in Bel-7402 cell(a), Hep3B cell(b), HepG2(c) and HL-7702(d) during 48, 72, and 96 h treatments with 12.5 μg ml^{-1} of FL/QD-TK and L/QD-TK with or without 10 μg ml^{-1} GCV measured by the MTT assay. The data represent three separate experiments. Mean values ± SD. *P < 0.05 *versus* control group, #P < 0.01 stands for FL/QD-TK *versus* L/QD-TK group.

L/QD-TK or the FL/QD-TK group after a 72 h GCV treatment. The FL/QD-TK/ GCV system showed a significant difference in Bel-7402 cells, rather than HepG2 cells; meanwhile, L/QD-TK, FL/QD-TK and GCV alone showed no cytotoxicity. FR-overexpressed Hep3B and SMMC-7721 cells as well as low FR-overexpression HL-7702 cells also employed the same experiments and confirmed the generality of the results.

To evaluate the theranostic efficacy of the FL/QD-TK/GCV system, the Bel-7402 xenograft was replicated in 30 nude mice. Six groups, including the control (only tumor inoculation), GCV alone, L/QD-TK alone, FL/QD-TK alone, L/QD-TK/GCV and FL/QD-TK/GCV, were tested with 5 mice in each group. Seven days after inoculation with Bel-7402 cells, the tumor-bearing nude mice were injected intravenously with liposomes every 3–4 days for a total of 6 administrations, and the experiment was concluded on the 26th day. For the L/QD-TK/GCV and FL/QD-TK/GCV groups, GCV i.p. injection was conducted 24 h post-administration of L/QD-TK or FL/QD-TK. The procedure is illustrated in Fig. 9a. The tumor volumes were measured after systemic administration of the liposomes. As shown in Fig. 9b, it is demonstrated that the FL/QD-TK/GCV group showed a significantly higher tumor inhibition rate of 90 ± 2.4%, compared to that of 73 ± 3.7% in the L/QD-TK/GCV group. Tumor inhibition effects were not observed in other groups. A comparison of tumor weight and appearance after excision also revealed that the therapeutic effect of FL/QD-TK/GCV was obviously better than that of L/QD-TK/GCV (Fig. 9c and d), which is consistent with more FL/QD-TK in the tumor tissue than the L/QD-TK detected by NIR QD. This indicated that the high tumor targeting ability of FL/QD-TK resulted in suppression of tumor growth because of its distribution in cancer tissue. All these aspects contributed to the superior therapeutic efficacy and the relative safety of FL/QD-TK for liver cancer treatment.

3.5 Biosafety evaluation of FL/QD-TK/GCV in mice

Safety profiling included the assessment of blood chemistry, total body weight and histological morphology of major organs. Compared to saline control tumor-bearing mice, no significant body weight changes were observed during the administration of either FL/QD-TK/GCV or free liposomes (Fig. 10d). In contrast, animals receiving L/QD-TK/GCV administration showed a cyclical decrease in body weight. Moreover, these animals also showed significant elevations of liver function enzymes aspartate aminotransferase (AST), as well as an increased kidney function marker blood urea nitrogen (BUN) values compared to the saline control and other groups (Fig. 10a, b and c). In addition, histological analysis of tissues from treated mice and control mice (Fig. 11) revealed no pathological changes in the heart, lung, kidney, liver or spleen. Interestingly, histological examination of tissue did not show any pathological changes in the L/QD-TK/GCV treated group. Although there are no short-term toxicological effects here, and other report found that these types of QDs are non-toxic as soon as they degraded in long-term experiments[50], clinical translation of such materials should be discreet. In summary, this study confirmed that theranostic liposomes could not only be applied for image-guided and targeted suicide gene therapy but could also reduce side effects and toxicity. It may provide a new strategy for real-time gene delivery and targeted cancer therapy.

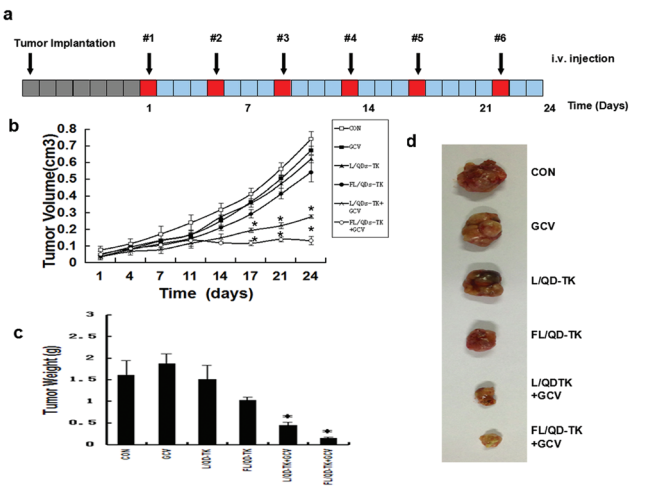

Fig. 9 Tumor growth inhibition effects of FL/QD-TK *in vivo*. (a) Bel-7402 cancer cells were subcutaneously injected into mice 7 days before treatment with FL/QD-TK (gray boxes). These animals received 6 i.v. injections (red boxes) every 3–4 days (blue boxes) for 26 days as shown. (b) Tumor growth inhibition in nude mice bearing Bel-7402 tumors after tail vein injection of different formulations. (c) Comparison of tumor weight of FL/QD-TK plus GCV *versus* other treatment groups: saline, GCV, L/QD-TK, FL/QD-TK and FL/QD-TK plus GCV (n = 6). (d) Photographs of collected tumor tissues for each treatment group. Mean values ± SD. *P < 0.05 *versus* control group.

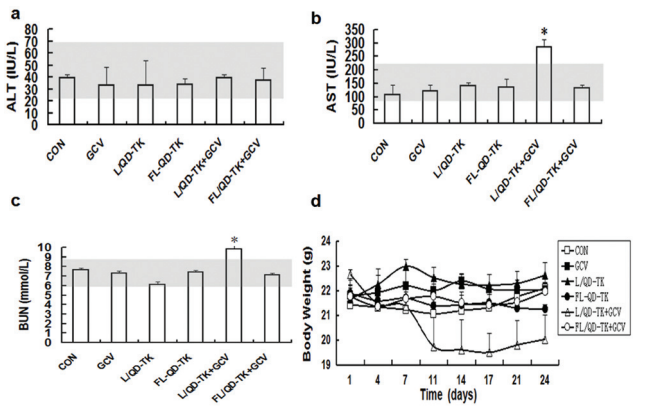

Fig. 10 Assessment of the systemic side effects of different treatments. Effect of different treatments on serum biochemistry at 26 days (n = 6), related serum biochemistry indicators include (a) alanine aminotransferase (ALT), (b) aspartate aminotransferase (AST), and (c) blood urea nitrogen (BUN). Gray bars indicate the range of values obtained from healthy nude mice. (d) The animal weights were recorded once in every three days and expressed over the 26-day observation period. Mean values ± SD. *P < 0.05 *versus* control group.

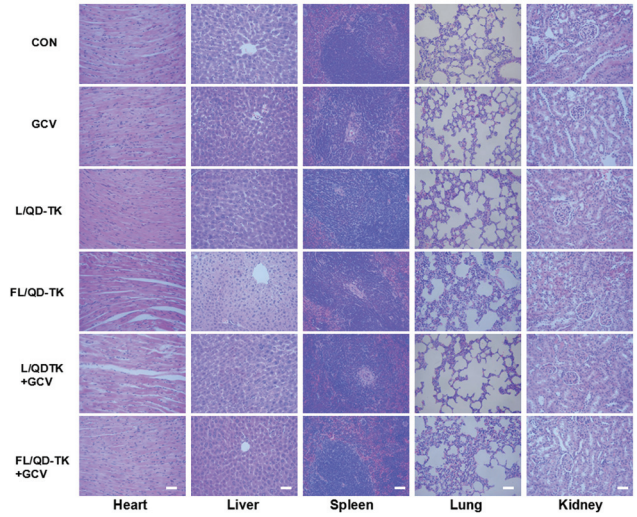

Fig. 11 Histological images from the major organs of the treated mice. Tissues were collected from brain, heart, liver, spleen, lung and kidney. Images were obtained at ×40 magnification with standard haematoxylin and eosin (HE) staining. Scale bars represent 50 μm.

4. Conclusions

In summary, we have successfully developed folate-targeting liposomes for the delivery of an HSV-TK suicide gene (FL/QD-TK). FL/QD-TK exhibited the capability of enhanced targeted delivery of the TK gene and real-time monitored temporal and spatial distribution of the TK gene *in vitro* and *in vivo*. In addition, FL/QD-TK had excellent therapeutic efficacy with minimal side effects, indicating that FL/QD-TK has potential advantages to overcome the problems of conventional suicide gene therapy and might be applied as a theranostic tool for real-time gene delivery and therapy in liver cancer.

Acknowledgements

Prof. Bai Yang, Prof. Xiang-gui Kong, Prof. Wen-fei Dong, Prof. Qing-hui Zeng, Dr Fang-zhong Shen, Dr Guang-fan Chi, Dr Ying-shuai Wang, Dr Shuang Li, Dr Qiong-shu Li, Dr Hai-jun Li, Dr Shuo Li, Dr Qi-hui Liu, Ou Li and Hui-lin Zheng are acknowledged for their help in preparing the paper. This work is sponsored by the National Natural Science Foundation of China (81071886, 81201804, 81371681), the Science and Technology Support Program of Jilin province (20090441, 201205006), and the Graduate Innovation Fund of Jilin University (20121118), the Opening Project of State Key Laboratory of Supramolecular Structure and Materials of Jilin University under grant no. SKLSSM 200912 and no. SKLSSM 201317. Most experiments were carried out at the Nanomedicine Engineering Laboratory of Jilin Province and Preclinical Pharmacology R&D Center of Jilin Province.

Notes and references

1 M. Maluccio and A. Covey, *CA-Cancer J. Clin.*, 2012, **62**, 394–399.
2 J. D. Yang and L. R. Roberts, *Nat. Rev. Gastroenterol. Hepatol.*, 2010, **7**, 448–458.
3 J. Bruix, G. J. Gores and V. Mazzaferro, *Gut*, 2014, **63**, 844–855.
4 J. Xie, S. Lee and X. Chen, *Adv. Drug Delivery Rev.*, 2010, **62**, 1064–1079.
5 T. Lammers, S. Aime, W. E. Hennink, G. Storm and F. Kiessling, *Acc. Chem. Res.*, 2011, **44**, 1029–1038.
6 B. Sumer and J. Gao, *Nanomedicine*, 2008, **3**, 137–140.
7 M. S. Muthu, D. T. Leong, L. Mei and S. S. Feng, *Theranostics*, 2014, **4**, 660–677.
8 S. Duarte, G. Carle, H. Faneca, M. C. de Lima and V. Pierrefite-Carle, *Cancer Lett.*, 2012, **324**, 160–170.
9 R. A. Morgan, *Mol. Ther.*, 2012, **20**, 11–13.
10 C. Fillat, M. Carrio, A. Cascante and B. Sangro, *Curr. Gene Ther.*, 2003, **3**, 13–26.
11 B. Sangro, G. Mazzolini, M. Ruiz, J. Ruiz, J. Quiroga, I. Herrero, C. Qian, A. Benito, J. Larrache, C. Olague, J. Boan, I. Penuelas, B. Sadaba and J. Prieto, *Cancer Gene Ther.*, 2010, **17**, 837–843.
12 H. A. Kim, K. Nam, M. Lee and S. W. Kim, *J. Controlled Release*, 2013, **171**, 1–10.
13 Y. Hasegawa, Y. Nishiyama, K. Imaizumi, N. Ono, T. Kinoshita, S. Hatano, H. Saito and K. Shimokata, *Cancer Gene Ther.*, 2000, **7**, 557–562.
14 Y. Terazaki, S. Yano, K. Yuge, S. Nagano, M. Fukunaga, Z. S. Guo, S. Komiya, K. Shirouzu and K. Kosai, *Hepatology*, 2003, **37**, 155–163.
15 P. L. Felgner and G. M. Ringold, *Nature*, 1989, **337**, 387–388.
16 P. P. Karmali and A. Chaudhuri, *Med. Res. Rev.*, 2007, **27**, 696–722.
17 W. T. Al-Jamal and K. Kostarelos, *Acc. Chem. Res.*, 2011, **44**, 1094–1104.
18 R. Pinyol and J. M. Llovet, *Nat. Rev. Gastroenterol. Hepatol.*, 2014, **11**, 336–337.
19 J. H. Maeng, D. H. Lee, K. H. Jung, Y. H. Bae, I. S. Park, S. Jeong, Y. S. Jeon, C. K. Shim, W. Kim, J. Kim, J. Lee, Y. M. Lee, J. H. Kim, W. H. Kim and S. S. Hong, *Biomaterials*, 2010, **31**, 4995–5006.
20 M. Wang, H. Hu, Y. Sun, L. Qiu, J. Zhang, G. Guan, X. Zhao, M. Qiao, L. Cheng and D. Chen, *Biomaterials*, 2013, **34**, 10120–10132.
21 Z. Xu, Z. Zhang, Y. Chen, L. Chen, L. Lin and Y. Li, *Biomaterials*, 2010, **31**, 916–922.
22 G. Liu, M. Swierczewska, S. Lee and X. Chen, *Nano Today*, 2010, **5**, 524–539.
23 K. C. Sia, H. Huynh, N. Chinnasamy, K. M. Hui and P. Y. Lam, *Gene Ther.*, 2012, **19**, 532–542.
24 X. Chen, *Nanoplatform-based molecular imaging*, Wiley Online Library, 2011.
25 M. A. Pysz, S. S. Gambhir and J. K. Willmann, *Clin. Radiol.*, 2010, **65**, 500–516.

26 Y. Waerzeggers, P. Monfared, T. Viel, A. Winkeler, J. Voges and A. H. Jacobs, *Methods*, 2009, **48**, 146–160.
27 W. K. Leutwyler, S. L. Bürgi and H. Burgl, *Science*, 1996, **271**, 933.
28 V. I. Klimov, A. A. Mikhailovsky, S. Xu, A. Malko, J. A. Hollingsworth, C. A. Leatherdale, H. Eisler and M. G. Bawendi, *Science*, 2000, **290**, 314–317.
29 P. Lodahl, A. Floris Van Driel, I. S. Nikolaev, A. Irman, K. Overgaag, D. Vanmaekelbergh and W. L. Vos, *Nature*, 2004, **430**, 654–657.
30 I. L. Medintz, H. T. Uyeda, E. R. Goldman and H. Mattoussi, *Nat. Mater.*, 2005, **4**, 435–446.
31 X. Michalet, F. F. Pinaud, L. A. Bentolila, J. M. Tsay, S. Doose, J. J. Li, G. Sundaresan, A. M. Wu, S. S. Gambhir and S. Weiss, *Science*, 2005, **307**, 538–544.
32 X. Gao, Y. Cui, R. M. Levenson, L. W. Chung and S. Nie, *Nat. Biotechnol.*, 2004, **22**, 969–976.
33 J. M. Li, Y. Y. Wang, M. X. Zhao, C. P. Tan, Y. Q. Li, X. Y. Le, L. N. Ji and Z. W. Mao, *Biomaterials*, 2012, **33**, 2780–2790.
34 Y. Li, X. Duan, L. Jing, C. Yang, R. Qiao and M. Gao, *Biomaterials*, 2011, **32**, 1923–1931.
35 C. E. Probst, P. Zrazhevskiy, V. Bagalkot and X. Gao, *Adv. Drug Delivery Rev.*, 2013, **65**, 703–718.
36 D. Shao, Q. Zeng, Z. Fan, J. Li, M. Zhang, Y. Zhang, O. Li, L. Chen, X. Kong and H. Zhang, *Biomaterials*, 2012, **33**, 4336–4344.
37 T. M. Allen and P. R. Cullis, *Adv. Drug Delivery Rev.*, 2013, **65**, 36–48.
38 M. Munoz-Ubeda, S. K. Misra, A. L. Barran-Berdon, C. Aicart-Ramos, M. B. Sierra, J. Biswas, P. Kondaiah, E. Junquera, S. Bhattacharya and E. Aicart, *JACS*, 2011, **133**, 18014–18017.
39 G. M. van Dam, G. Themelis, L. M. Crane, N. J. Harlaar, R. G. Pleijhuis, W. Kelder, A. Sarantopoulos, J. S. de Jong, H. J. Arts, A. G. van der Zee, J. Bart, P. S. Low and V. Ntziachristos, *Nat. Med.*, 2011, **17**, 1315–1319.
40 C. L. Walters, R. C. Arend, D. K. Armstrong, R. W. Naumann and R. D. Alvarez, *Gynecol. Oncol.*, 2013, **131**, 493–498.
41 Y. Lu and P. S. Low, *Adv. Drug Delivery Rev.*, 2002, **54**, 675–693.
42 P. S. Low, W. A. Henne and D. D. Doorneweerd, *Acc. Chem. Res.*, 2008, **41**, 120–129.
43 K. Maruyama, *Adv. Drug Delivery Rev.*, 2011, **63**, 161–169.
44 R. T. Proffitt, L. E. Williams, C. A. Presant, G. W. Tin, J. A. Uliana, R. C. Gamble and J. D. Baldeschwieler, *Science*, 1983, **220**, 502–505.
45 Y. Zhuang, Y. Ma, C. Wang, L. Hai, C. Yan, Y. Zhang, F. Liu and L. Cai, *J. Controlled Release*, 2012, **159**, 135–142.
46 S. Kuriyama, M. Kikukawa, K. Masui, H. Okuda, T. Nakatani, T. Akahane, A. Mitoro, K. Tominaga, H. Tsujinoue, H. Yoshiji, S. Okamoto, H. Fukui and K. Ikenaka, *Int. J. Cancer*, 1999, **83**, 374–380.
47 T. U. Krohne, S. Shankara, M. Geissler, B. L. Roberts, J. R. Wands, H. E. Blum and L. Mohr, *Hepatology*, 2001, **34**, 511–518.
48 E. Preuss, A. Muik, K. Weber, J. Otte, D. von Laer and B. Fehse, *J. Mol. Med.*, 2011, **89**, 1113–1124.
49 A. Neschadim, J. C. Wang, A. Lavie and J. A. Medin, *Cancer Gene Ther.*, 2012, **19**, 320–327.
50 L. Ye, K. T. Yong, L. Liu, I. Roy, R. Hu, J. Zhu, H. Cai, W. C. Law, J. Liu, K. Wang, Y. Liu, Y. Hu, X. Zhang, M. T. Swihart and P. N. Prasad, *Nat. Nanotechnol.*, 2012, **7**, 453–458.